Supplementary data to
A four state parametric model for the kinetics of the non-photochemical quenching in Photosystem II

Joris J. Snellenburg[a], Matthew P. Johnson [b], Alexander V. Ruban[c], Rienk van Grondelle[a], Ivo H.M. van Stokkum*[a]

[a] Institute for Lasers, Life and Biophotonics, Faculty of Sciences, VU University Amsterdam, De Boelelaan 1081, 1081 HV, Amsterdam, The Netherlands.

[b] Department of Molecular Biology and Biotechnology, University of Sheffield, UK
[c] School of Biological and Chemical Sciences, Queen Mary University of London, UK

Contents

Components of a parametric model for PAM curves

This section contains a detailed specification of the function required to fit the PAM quenching analysis curves measured from intact chloroplasts. The fitting function takes into account the possible contributions to the observed chlorophyll fluorescence quantum yield from the supercomplexes Photosystem II (PSII) and Photosystem I (PSI) and (disconnected) Light Harvesting Complex II (LHCII). Here the PSII contribution is assumed to be a linear superposition of four possible states, each with a unique quantum yield, related to the state of the PSII RC (open or closed) and the rate of non-photochemical quenching of the PSII supercomplex. Other contributions such as from disconnected Chlorophyll molecules, different chromophores such as phycobilins (relevant for the measured fluorescence in Cyanobacteria [1] or specific experimentally related background contributions are not included in this specification, but can easily be included if needed. Considering the large number of contributions to the fitting function, it is important to keep the specification as concise as possible. A compact way to list the contributions to the fitting function for a particular pigment-protein complex is using the tensor product (also called outer product) of its independent state vectors:

$$\{o,c\} \otimes \{u,q\} = \{\{ou, oq\}, \{cu, cq\}\} \qquad \text{Eq.S1}$$

The product ***cq*** then represents the function that describes the concentration of PSII in the closed, quenched state. For the total contribution J to the PAM signal each concentration function still needs to be multiplied with its quantum yield

Φ_{kl}^{j}, where the additional indices *k* and *l* represent different light–acclimated states; in the case of PSII *k* takes into account whether the state is open or closed and *l* stands for either a quenched or an unquenched species. This can be achieved by taking the result of the tensor product, flattening the 2 dimensional tensor in a column wise manner $\{ou, oq, cu, cq\}$ and then taking the inner product with the respective yield parameters. This operation is abbreviated using a helper function termed outer product function (OPF), with an additional label to indicate which species it describes. For PSII this is written as:

$$\begin{aligned} J^{PSII} &= OPF^{PSII}\left[\{o,c\},\{u,q\}\right] = OPF\left[\left\{\Phi_{ou}^{PSII},\Phi_{oq}^{PSII},\Phi_{cu}^{PSII},\Phi_{cq}^{PSII}\right\},\left\{\{o,c\},\{u,q\}\right\}\right] = \\ & ou\Phi_{ou}^{PSII} + oq\Phi_{oq}^{PSII} + cu\Phi_{cu}^{PSII} + cq\Phi_{cq}^{PSII} \end{aligned} \quad \text{Eq.S2}$$

And for LHCII, which only occurs in quenched or unquenched form, this is written as:

$$\begin{aligned} J^{LHCII} &= OPF^{LHCII}\left[\{u,q\}\right] = OPF\left[\left\{\Phi_{u}^{LHCII},\Phi_{q}^{LHCII}\right\},\left\{\{u,q\}\right\}\right] = \\ & u\Phi_{u}^{LHCII}, q\Phi_{q}^{LHCII} \end{aligned} \quad \text{Eq.S3}$$

In the case of the contribution from PSI the most compact notation is simply the product of concentration and quantum yield:

$$J^{PSI} = c_{PSI}\Phi^{PSI} \quad \text{Eq.S4}$$

Finally it is necessary to account for the stoichiometry between the contributions using fractional parameters, e.g. for PSII, LHCII and PSI respectively $(1 - fr_{LHCII})$, fr_{LHCII} and fr_{PSI}. This is necessary to account for the relative stoichiometry of the proteins themselves, but also to account for the relative difference in absorption at the excitation wavelength used to excite the sample. In this way, when the contribution of PSI and disconnected LHCII can be neglected the fractional constant is just 1. In the case that PSI can be neglected but there is a fair amount of disconnected LHCII then the fraction also sums up to 1.

In the follow paragraphs the exact equations used to construct the fitting function are listed clustered per light regime (dark adapted sample, quenching inducing high light following darkness, recovery in darkness following high light) and given a label so that they can be referenced in subsequent function definitions using the notation BFS["function_label"], where BFS refers to "Basis Function Set". Below the equations are subsequently explained in the order of the light conditions in the experiment described in the main text (see section "Analyzing a full PAM quenching curve" and **Figure 2**)

Darkness (da)

In the region where there is only measuring light and no source of actinic light, the Photosystem II (PSII) reaction centers (RCs) are assumed to be in the open state. If the sample is also dark adapted (has not seen any strong source of actinic light for a long enough period of time) it is also unquenched. Under these light conditions PSII has a fluorescence quantum yield Φ_{ou}^{PSII}. However at the same time it is possible to have contributions to the total signal of unconnected Light Harvesting Complex II (LHCII) and Photosystem I (PSI). This can then be summarized in the equation for a dark adapted ("da") segment:

$$\text{"da"} \rightarrow (1 - fr_{LHCII})\Phi_{ou}^{PSII} + fr_{LHCII}\Phi_{u}^{LHCII} + fr_{PSI}\Phi^{PSI} \quad \text{Eq.S5}$$

The next change in light conditions is a saturation pulse applied at time t_0, with the continuous actinic light source still switched off. To describe the sudden rise in measured fluorescence quantum yield, due to the closing of PSII RC's, a mono exponential function is used "dkspIRF" with rate constant k_1. The subsequent recovery toward the level where all PSII RC's are again open is modeled using three exponential decays (rate constants k_2, k_3, k_{3b}).

$$\text{"dkspIRF"} \rightarrow e^{-k_1^L(t-t_0)}, \text{"dkspD1"} \rightarrow e^{-k_2^L(t-t_0)}, \text{"dkspD2"} \rightarrow e^{-k_3^L(t-t_0)}, \text{"dkspD2b"} \rightarrow e^{-k_{3b}^L(t-t_0)} \quad \text{Eq.S6}$$

Here L represents a label to distinguish the parameters for the same function used in different light conditions. The same functional description can then be used to describe the effect of a specific change in light conditions (e.g. a saturating pulse in darkness) but observed differences in kinetics can then be taken into account by freeing some

parameters. The data described in the main manuscript required freeing the rate k_3 between the first two saturating pulses in darkness for a dark acclimated sample, and the remaining saturating pulses in darkness for a sample that had already been exposed to high light. Then for the first two saturation pulses in darkness k_3 is then defined as k_3^{SP1} and for the rest the parameter k_3^{D1} is used. The rates k_2^{D1}, k_{3b}^{D1} are the same (linked) throughout.

A careful reader might notice that the fluorescence induction dynamics and subsequent relaxation is captured using just a few exponentials, implying underlying first order differential equations. This is a strong assumption but not a necessary one. If more information is available on the dynamics of a particular transition this a priori knowledge can be used to refine the components of the fit function.

With the above definitions the rise of the fluorescence in darkness can be written as:

$$\text{"dkspR"} \rightarrow (1 - fr_{\text{LHCII}})\,\text{OPF}\left[\left\{\begin{matrix}\Phi_{\text{ou}}^{\text{PSII}},\\ \Phi_{\text{cu}}^{\text{PSII}}\end{matrix}\right\}, \left\{\left\{\begin{matrix}\text{BFS}[\text{"dkspIRF"}],\\ 1-\text{BFS}[\text{"dkspIRF"}]\end{matrix}\right\}\right\}\right] + fr_{\text{LHCII}}\Phi_{\text{u}}^{\text{LHCII}} + fr_{\text{PSI}}\Phi^{\text{PSI}} \qquad \text{Eq.S7}$$

The subsequent decay is then described as:

$$\begin{aligned}\text{"dkspD"} \rightarrow (1 - fr_{\text{LHCII}})\,\text{OPF}&\left[\left\{\begin{matrix}\Phi_{\text{ou}}^{\text{PSII}},\\ \Phi_{\text{cu}}^{\text{PSII}}\end{matrix}\right\}, \left\{\left\{\begin{matrix}\left(\begin{matrix}fr_2^{\text{L}}\left(1-\text{BFS}[\text{"dkspD1"}]\right)+\\ \left(1-fr_{3\text{b}}^{\text{L}}\right)\left(1-fr_2^{\text{L}}\right)\left(1-\text{BFS}[\text{"dkspD2"}]\right)+\\ fr_{3\text{b}}^{\text{L}}\left(1-fr_2^{\text{L}}\right)*\left(1-\text{BFS}[\text{"dkspD2b"}]\right)\end{matrix}\right),\\ \left(\begin{matrix}fr_2^{\text{L}}*BFS[\text{"dkspD1"}]+\\ \left(1-fr_{3\text{b}}^{\text{L}}\right)*\left(1-fr_2^{\text{L}}\right)*\text{BFS}[\text{"dkspD2"}]+\\ fr_{3\text{b}}^{\text{L}}*\left(1-fr_2^{\text{L}}\right)*\text{BFS}[\text{"dkspD2b"}]\end{matrix}\right)\end{matrix}\right\}\right]\right]\\ &+ fr_{\text{LHCII}}\Phi_{\text{u}}^{\text{LHCII}} + fr_{\text{PSI}}\Phi^{\text{PSI}}\end{aligned} \qquad \text{Eq.S8}$$

Where the fractional parameters $fr_2^{\text{L}}, fr_{3\text{b}}^{\text{L}}$ are introduced to express the amplitudes of the exponential decays of Eq.S6. For the first two periods of darkness these parameters are defined as $fr_2^{D1}, fr_{3\text{b}}^{D1}$, expect for the first saturating pulse which uses $fr_2^{SP1}, fr_{3\text{b}}^{SP1}$.

Darkness to high light (dk2hl)

When a period of (high) continuous actinic light follows a period of darkness a number of additional function definitions are needed. First the function "dkendC" evaluates the function "dkspD" for the time point just before the dark to light transition t_{LR1end} and quantifies the amount of closed PSII left over due to only partial recovery from a saturating pulse in darkness.

$$\text{"dkendC"} \rightarrow \text{BFS}[\text{"dkspD"}] \text{ with } t \rightarrow t_{LR1end} \qquad \text{Eq.S9}$$

The fluorescence induction dynamics due to the continuous actinic light is again described using a single exponential, but with a different rate constant.

$$\text{"dkhlIRF"} \rightarrow e^{-k_{10}^{L}(t-t_0)} \qquad \text{Eq.S10}$$

Assuming that upon switching to continuous light all the PSII RCs are closed, a small fraction (depending on the absolute level of light intensity) of the RCs can again re-open if the excitation pressure is not enough to keep them completely closed, which is accounted for using a single exponential, where a certain fraction $\left(1 - fr_{\text{CC}}^{\text{H1}}\right)$ of the PSII RCs reopens. The amount of closed PSII can then be described as

$$\text{"hlPSIIc"} \rightarrow \left(1 - fr_{CC}^{H1}\right) e^{-k_6 (t - t_{LLR})} + fr_{CC}^{H1} \qquad \text{Eq.S11}$$

where t_{LLR} is substituted with the timepoint of the last light regime (thus $(t - t_{LLR})$ is the time since switching on the actinic light). The amount of open PSII RCs is simply one minus the closed concentration.

$$\text{"hlPSIIo"} \rightarrow 1 - \text{BFS}[\text{"hlPSIIc"}] \qquad \text{Eq.S12}$$

Using these function definitions the amount of PSII closed/open in the darkness to high light transition can be written as

$$\begin{gathered} \text{"dk2hlPSIIc"} \rightarrow \text{BFS}[\text{"dkendC"}] + \left(1 - \text{BFS}[\text{"dkendC"}]\right) \text{BFS}[\text{"hlPSIIc"}] \left(1 - \text{BFS}[\text{"dkhlIRF"}]\right) \\ \text{"dk2hlPSIIo"} \rightarrow 1 - \text{BFS}[\text{"dk2hlPSIIc"}] \end{gathered} \qquad \text{Eq.S13}$$

During a period of high light non-photochemical quenching is induced, leading to a lower observed fluorescence quantum yield. This is captured in a quenching function which describes the decay of the unquenched population.

To account for a small fraction of initially quenched PSII we define two functions. A fraction fr_{isq} which can be a left over from a previous partial recovery, and a fraction fr_{ifq} due to very fast quenching unresolvable given the limited time-resolution of the experiment (60ms time steps in this case).

$$\text{"ISQ"} \rightarrow fr_{isq}^{L}, \text{"IFQ"} \rightarrow fr_{ifq}^{L} \qquad \text{Eq.S14}$$

Out of the total amount that can be quenched fr_{Q}^{H1} a certain fraction is associated with a relatively slow recovery and therefore indicated with the label "SQ": fr_{SQ}^{H1}, described by a single exponential. Another fraction recovers relatively quickly "FQ": $1 - fr_{SQ}^{H1}$, and can be fitted as the sum of 2 exponentials.

$$\begin{aligned} \text{"hlUnQS"} &\rightarrow \left(1 - \text{BFS}[\text{"ISQ"}]\right) fr_{SQ}\, e^{-k_{4a}^{H1}\left(t - t_{LR\_1}\right)} \\ \text{"hlUnQF"} &\rightarrow \left(1 - \text{BFS}[\text{"IFQ"}]\right)\left(fr_4^{H1}\, e^{-k_4^{H1}\left(t - t_{LR\_1}\right)} + \left(1 - fr_4^{H1}\right) e^{-k_5^{H1}\left(t - t_{LR\_1}\right)} \right) \end{aligned} \qquad \text{Eq.S15}$$

The total function for the relative amount of unquenched and quenched concentration is then written as:

$$\begin{gathered} \text{"hlUnQ"} \rightarrow \left(1 - fr_Q\right) + fr_Q * \left(fr_{SQ}\, \text{BFS}[\text{"hlUnQS"}] + \left(1 - fr_{SQ}\right) \text{BFS}[\text{"hlUnQF"}] \right) \\ \text{"hlQ"} \rightarrow 1 - \text{BFS}[\text{"hlUnQ"}] \end{gathered} \qquad \text{Eq.S16}$$

The full expression to describe the darkness to high light transition can now be assembled:

$$\begin{aligned} \text{"dk2hl"} \rightarrow \left(1 - fr_{LHCII}\right) \text{OPF}^{PSII} \left[\begin{Bmatrix} \left\{ \left(\text{BFS}[\text{"dk2hlPSIIo"}]\right), \text{BFS}[\text{"dk2hlPSIIc"}] \right\}, \\ \left\{ \text{BFS}[\text{"hlQ"}], \text{BFS}[\text{"hlUnQ"}] \right\} \end{Bmatrix} \right] + \\ fr_{LHCII}\, \text{OPF}^{LHCII} \left[\left\{ \left\{ \text{BFS}[\text{"hlQ"}], \text{BFS}[\text{"hlUnQ"}] \right\} \right\} \right] + fr_{PSI} \Phi^{PSI} \end{aligned} \qquad \text{Eq.S17}$$

During the period of continuous actinic light, there are also periodically saturating pulses given to ensure that all PSII RCs are fully closed. The necessary function to fit this aspect in the data is similar to the saturating pulses applied during darkness expect that the kinetics is much faster and both the rise and decay can be fitted with a single exponential.

$$\text{"hlspIRF"} \to e^{-k_1^{H1}(t-t_0)} \text{ , "hlspD1"} \to e^{-k_2^{H1}(t-t_0)} \qquad \text{Eq.S18}$$

This then leads to the amount of open/closed PSII during a saturating pulse during high light being described by:

$$\begin{aligned} \text{"hlspPSIIo"} &\to \text{BFS}[\text{"hlspIRF"}]\left(1-\text{BFS}[\text{"hlPSIIc"}]\right) \\ \text{"hlspPSIIc"} &\to \text{BFS}[\text{"hlPSIIc"}]+\left(1-\text{BFS}[\text{"hlspIRF"}]\right)\left(1-\text{BFS}[\text{"hlPSIIc"}]\right) \end{aligned} \qquad \text{Eq.S19}$$

When the above function definitions are combined the expression for the rise and decay of fluorescence yield during actinic light can respectively be written as:

$$\begin{aligned} \text{"hlspR"} \to \left(1- fr_{\text{LHCII}}\right)\text{OPF}^{\text{PSII}} &\left[\begin{Bmatrix}\{\left(\text{BFS}[\text{"hlspPSIIo"}]\right),\text{BFS}[\text{"hlspPSIIc"}]\},\\ \{\text{BFS}[\text{"hlQ"}],\text{BFS}[\text{"hlUnQ"}]\}\end{Bmatrix}\right]+ \\ fr_{\text{LHCII}}\,\text{OPF}^{\text{LHCII}}&\left[\{\{\text{BFS}[\text{"hlQ"}],\text{BFS}[\text{"hlUnQ"}]\}\}\right]+ fr_{\text{PSI}}\Phi^{\text{PSI}} \end{aligned} \qquad \text{Eq.S20}$$

$$\begin{aligned} \text{"hlspD"}->\left(1- fr_{\text{LHCII}}\right)\text{OPF}^{\text{PSII}} &\left[\begin{Bmatrix}\{\left(\left(1-\text{BFS}[\text{"hlspD1"}]\right)\text{BFS}[\text{"hlPSIIo"}]\right),\\ \left(1-\text{BFS}[\text{"hlPSIIc"}]\right)\text{BFS}[\text{"hlspD1"}]+\text{BFS}[\text{"hlPSIIc"}]\}\\ \{\text{BFS}[\text{"hlQ"}],\text{BFS}[\text{"hlUnQ"}]\}\end{Bmatrix},\right]+ \\ fr_{\text{LHCII}}\,\text{OPF}^{\text{LHCII}}&\left[\{\{\text{BFS}[\text{"hlQ"}],\text{BFS}[\text{"hlUnQ"}]\}\}\right]+ fr_{\text{PSI}}\Phi^{\text{PSI}} \end{aligned} \qquad \text{Eq.S21}$$

High light to darkness or recovery (hl2dk)

In a period of darkness, following actinic light, the induced non-photochemical quenching gradually recovers. The starting point for the recovery can be determined by evaluating the quenching function at the end of the high light period, just before the recovery period.

$$\begin{aligned} \text{"SQT"} &\to \left(1-\text{BFS}[\text{"hlUnQS"}]\right)\text{with } t-t_{\text{LR\_1}} \to t_{\text{LR\_1}}-t_{\text{LR\_2}} \\ \text{"FQT"} &\to \left(1-\text{BFS}[\text{"hlUnQF"}]\right)\text{with } t-t_{\text{LR\_1}} \to t_{\text{LR\_1}}-t_{\text{LR\_2}} \end{aligned} \qquad \text{Eq.S22}$$

The dynamics of recovery consists of two parts both fitted with a single exponential. One part of the induced quenching is recovered from very slowly ($fr_{\text{SQ}}^{\text{H1}}$) given by rate k_{8a}, while the other part recovers quickly $\left(1- fr_{\text{SQ}}^{\text{H1}}\right)$ given by rate k_8.

$$\begin{aligned} \text{"hldkRecF"} &\to \left(1-e^{-k_8^{\text{R1}}\left(t-t_{\text{LR\_1}}\right)}\right)\text{ , "hldkRecS"} \to \left(1-e^{-k_{8a}^{\text{R1}}\left(t-t_{\text{LR\_1}}\right)}\right), \\ \text{"hldkRec"} &\to fr_{\text{Q}}^{\text{H1}}\left(fr_{\text{SQ}}^{\text{H1}}\,\text{BFS}[\text{"hldkRecS"}])+\left(1- fr_{\text{SQ}}^{\text{H1}}\right)\text{BFS}[\text{"hldkRecF"}]\right), \end{aligned} \qquad \text{Eq.S23}$$

While recovery from NPQ is a relatively slow process, the reopening of PSII RCs is quite fast and results in a quick transition from mostly closed PSII RCs in actinic light, to completely open RCs in the recovery phase. The dynamics of this transition is captured by the same function which describes reopening after a saturating pulse.

$$\begin{aligned} \text{"hl2dkPSIIo"} \to\ & fr_2^{\text{L}}\left(1-\text{BFS}[\text{"dkspD1"}]\right)+\left(1- fr_{3\text{b}}^{\text{L}}\right)\left(1- fr_2^{\text{L}}\right)\left(1-\text{BFS}[\text{"dkspD2"}]\right)+ \\ & fr_{3\text{b}}^{\text{L}}\left(1- fr_2^{\text{L}}\right)*\left(1-\text{BFS}[\text{"dkspD2b"}]\right) \\ \text{"hl2dkPSIIc"} \to\ & fr_2^{\text{L}}\,BFS\left[\text{"dkspD1"}\right]+\left(1- fr_{3\text{b}}^{\text{L}}\right)\left(1- fr_2^{\text{L}}\right)\text{BFS}[\text{"dkspD2"}]+ \\ & fr_{3\text{b}}^{\text{L}}\left(1- fr_2^{\text{L}}\right)*\left(\text{BFS}[\text{"dkspD2b"}]\right) \end{aligned} \qquad \text{Eq.S24}$$

With fr_2^{L}, $fr_{3\text{b}}^{\text{L}}$ equal to fr_2^{D1}, $fr_{3\text{b}}^{\text{D1}}$ during the first recovery period and fr_2^{R2}, $fr_{3\text{b}}^{\text{R2}}$ during the second recovery period.

Finally the amount of unquenched and quenched PSII can then be expressed as:

$$
\begin{aligned}
\text{"hl2dkPSIIuS"} &\to \left(\left(1-\text{BFS}\left[\text{"SQT"}\right]\right)+\text{BFS}\left[\text{"SQT"}\right]\text{BFS}\left[\text{"hldkRecS"}\right]\right),\\
\text{"hl2dkPSIIuF"} &\to \left(\left(1-\text{BFS}\left[\text{"FQT"}\right]\right)+\text{BFS}\left[\text{"FQT"}\right]\text{BFS}\left[\text{"hldkRecF"}\right]\right),\\
\text{"hl2dkPSIIu"} &\to fr_{\text{Q}}\left(\left(1-fr_{\text{SQ}}\right)\text{BFS}\left[\text{"hl2dkPSIIuF"}\right]+fr_{\text{SQ}}\,\text{BFS}\left[\text{"hl2dkPSIIuS"}\right]\right),\\
\text{"hl2dkPSIIq"} &\to 1-\text{BFS}\left[\text{"hl2dkPSIIu"}\right],
\end{aligned}
\qquad \text{Eq.S25}
$$

The function definition that describes the quenching of LHCII can be postulated in the same way, but is not specified here in detail as there is no data in the main text to test it against. In a first approximation the quenching dynamics can be assumed to be the same as for the LHCII-PSII complex. When these functions are combined the function that described the transition from darkness to high light can be written as:

$$
\begin{aligned}
\text{"dk2hl"} \to{}& \left(1-fr_{\text{LHCII}}\right)\text{OPF}^{\text{PSII}}\left[\begin{Bmatrix}\left\{\left(\text{BFS}\left[\text{"hl2dkPSIIo"}\right]\right),\text{BFS}\left[\text{"hl2dkPSIIc"}\right]\right\},\\ \left\{\text{BFS}\left[\text{"hl2dkPSIIq"}\right],\text{BFS}\left[\text{"hl2dkPSIIu"}\right]\right\}\end{Bmatrix}\right]+\\
& fr_{\text{LHCII}}\,\text{OPF}^{\text{LHCII}}\left[\left\{\left\{\text{BFS}\left[\text{"hl2dkLHCIIq"}\right],\text{BFS}\left[\text{"hl2dkLHCIIu"}\right]\right\}\right\}\right]+fr_{\text{PSI}}\Phi^{\text{PSI}}
\end{aligned}
\qquad \text{Eq.S26}
$$

The rise of fluorescence due to a saturating pulse in darkness, taking into account the baseline level of recovery can be written as:

$$
\begin{aligned}
\text{"recPSIIc"} &\to \left(1-\text{BFS}\left[\text{"hl2dkPSIIc"}\right]\right)\left(1-\text{BFS}\left[\text{"dkspIRF"}\right]\right)+\text{BFS}\left[\text{"hl2dkPSIIc"}\right]\\
\text{"recPSIIo"} &\to 1-\text{BFS}\left[\text{"recPSIIc"}\right]
\end{aligned}
\qquad \text{Eq.S27}
$$

Finally making use of the above function definitions, the function that describe the segments in the recovery regime during and between saturating pulses can be formulated as:

$$
\begin{aligned}
\text{"recspR"} \to{}& \left(1-fr_{\text{LHCII}}\right)\text{OPF}^{\text{PSII}}\left[\begin{Bmatrix}\left\{\text{BFS}\left[\text{"recPSIIo"}\right],\text{BFS}\left[\text{"recPSIIc"}\right]\right\},\\ \left\{\text{BFS}\left[\text{"hl2dkPSIIq"}\right],\text{BFS}\left[\text{"hl2dkPSIIu"}\right]\right\}\end{Bmatrix}\right]+\\
& fr_{\text{LHCII}}\,\text{OPF}^{\text{LHCII}}\left[\left\{\left\{\text{BFS}\left[\text{"hl2dkLHCIIq"}\right],\text{BFS}\left[\text{"hl2dkLHCIIu"}\right]\right\}\right\}\right]+fr_{\text{PSI}}\Phi^{\text{PSI}}\\
\text{"recspD"} \to{}& \left(1-fr_{\text{LHCII}}\right)\text{OPF}^{\text{PSII}}\left[\begin{Bmatrix}\left\{\left\{\left(\text{BFS}\left[\text{"hl2dkPSIIo"}\right]\right),\left(\text{BFS}\left[\text{"hl2dkPSIIc"}\right]\right)\right\},\\ \left\{\text{BFS}\left[\text{"hl2dkPSIIq"}\right],\text{BFS}\left[\text{"hl2dkPSIIu"}\right]\right\}\end{Bmatrix}\right]+\\
& fr_{\text{LHCII}}\,\text{OPF}^{\text{LHCII}}\left[\left\{\left\{\text{BFS}\left[\text{"hl2dkLHCIIq"}\right],\text{BFS}\left[\text{"hl2dkLHCIIu"}\right]\right\}\right\}\right]+fr_{\text{PSI}}\Phi^{\text{PSI}}
\end{aligned}
\qquad \text{Eq.S28}
$$

Together these labeled functions can be used to model all the different changes in light conditions that are observed in the data reported in the main text.

Working model for the sample devoid of zeaxanthin

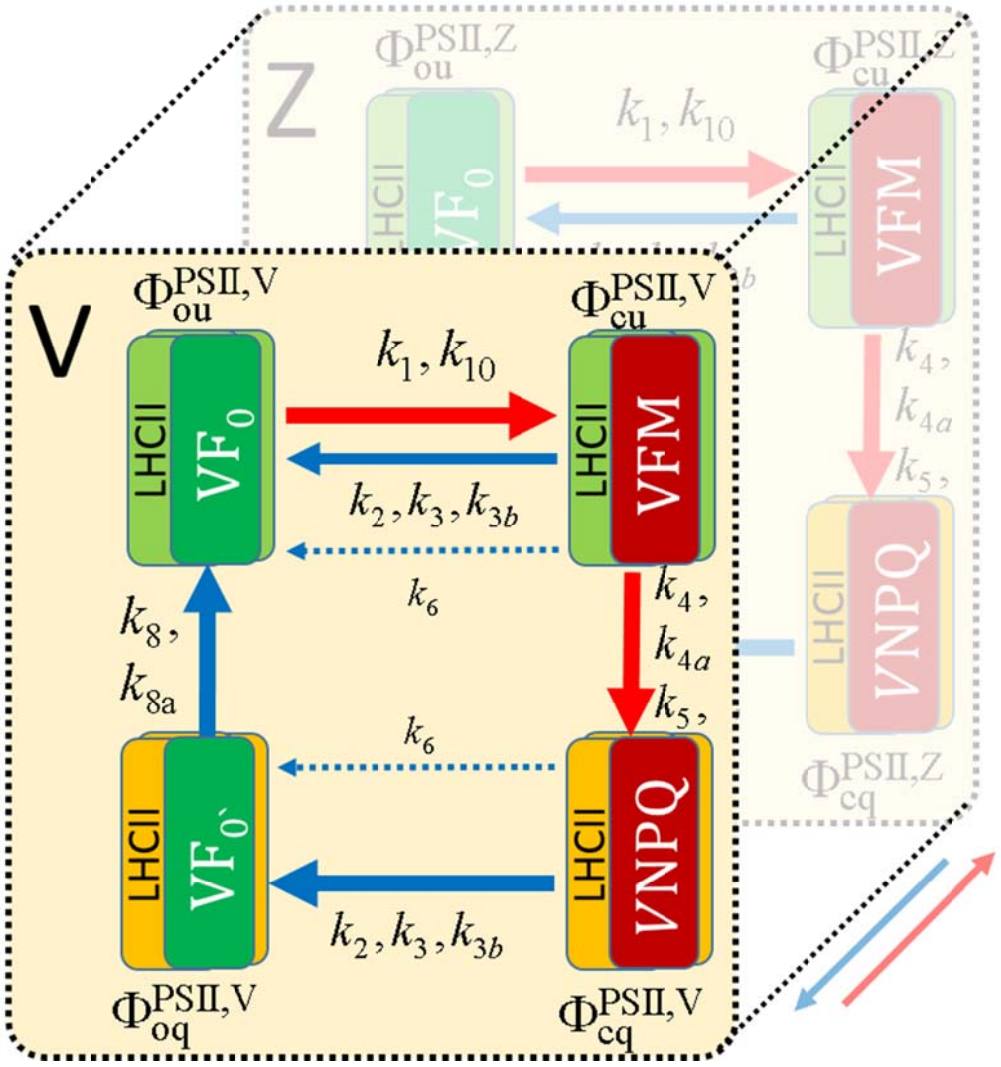

Figure S 1. Working mathematical model which ties the different species listed in Figure 1 to the parametric description given in equation (2) for the sample devoid of zeaxanthin (V). The premise of the model are four distinct states which can be interconverted into one another with certain rates, either light driven (red arrows) or spontaneously in the absence of light (blue arrows). The difference with the model for the Z case is an additional rate k_6 which represents re-opening of the reaction centers due to insufficient actinic light pressure to keep them completely closed. A simplification of the model is the assumption that the sample remains devoid of zeaxanthin over the course of the measurement.

Segments	Label	Description	Parameters introduced
1,2[1]	"bg"	Background signal, measuring light (ML) OFF	
3	"da"	Signal from a dark adapted sample (ML ON)	Φ_{ou}^{PSII}; $fr_{LHCII}, \Phi_{u}^{LHCII}$; fr_{PSI}, Φ^{PSI}
4,6	"dkspR"	Saturating pulse *rise* in darkness	Φ_{cu}^{PSII}, k_1^{D1}
5,7,8[1]	"dkspD"	Saturating pulse *decay* in darkness	$k_2^{D1}, k_3^{D1}, k_{3b}^{D1}, fr_2^{D1}, fr_{3b}^{D1}$, optionally $fr_2^{SP1}, fr_{3b}^{SP1}, k_3^{SP1}$
9	"dk2hl" (1)	Darkness to (high) actinic light	$\Phi_{oq}^{PSII}, \Phi_{cq}^{PSII}, fr_Q^{H1}, fr_{SQ}^{H1}, fr_4^{H1}, k_4^{H1}, k_5^{H1}, k_{10}^{D1}, fr_{CC}^{H1}, k_6^{H1}; \Phi_q^{LHCII}$
10,12,…,22	"hlspR" (1)	Saturating pulse *rise* in actinic light	k_1^{H1}
11,13,…,23	"hlspD" (1)	Saturating pulse *decay* in actinic light	k_2^{H1}
24[1],25	"hl2dk" (1)	Actinic light to darkness transition	k_8^{R1}, k_{8a}^{R1}, optionally fr_2^{R1}, fr_{3b}^{R1}
26,28,…,38	"recspR" (1)	Saturating pulse *rise* in darkness during recovery	
27,29,…39,40[1]	"recspD" (1)	Saturating pulse *decay* in darkness during recovery	
41	"dk2hl" (2)	Darkness to (high) actinic light (after recovery)	optionally $fr_4^{H2}, k_4^{H2}, k_5^{H2}$ and k_6^{H2}
42,44,…58	"hlspR" (2)	Saturating pulse *rise* in actinic light (after recovery)	
43,45,…59	"hlspD" (2)	Saturating pulse *decay* in actinic light (after recovery)	
60[1],61	"hl2dk" (2)	2nd Actinic light to darkness transition	optionally fr_2^{R2}, fr_{3b}^{R2}
62,64,…,74	"recspR" (2)	Saturating pulse *rise* in darkness during 2nd recovery	
63,65,…,75,76[1]	"recspD" (2)	Saturating pulse *decay* in darkness during 2nd recovery	
77	"bg"	Background signal after turning ML OFF.	

Table S 1: Full parameter table for the total fitting function for the 77 segments of the data. For each label a closed form expression is available in the present section. Labels (1) and (2) signify the first and second time a particular expression is used, for which the estimated parameters can have different numerical values. All parameters introduced for a function in a particular segment can be optionally made free in repeated occurrences of that function for subsequent segments. Specifically some parameters are listed here explicitly because they were freed in fitting one of the datasets described in the main text.

For SP1 $a_2 = fr_2^{SP1}, a_3 = \left(1-fr_{3b}^{SP1}\right)\left(1-fr_2^{SP1}\right), a_{3b} = fr_{3b}^{SP1}\left(1-fr_2^{SP1}\right)$

For SP2 $a_2 = fr_2^{D1}, a_3 = \left(1-fr_{3b}^{D1}\right)\left(1-fr_2^{D1}\right), a_{3b} = fr_{3b}^{D1}\left(1-fr_2^{D1}\right)$

Table S 2. Relation between amplitude parameters used in the main text and fractions given in **Table S 1**.

[1] These segments consist of only a single data point, between the end of one light regime and the start of the next. To describe this one transition point, the function of the previous or the next light regime is reused. This is a mechanism to deal with non-instantaneous light switching, although for the data reported in this simulation the switching occurred within the 60 ms time steps of the data.

```
In[222]:= Clear[xFrom, xTo, step];
          With[
           {args = Delete[parameterListZ, 0],
            controls = Join[parameterSettingsZ, {"Manipulate settings:", {{xFrom, 1}, 1, Length[r_timesZ] - 1}, {{xTo, Length[r_timesZ]}, 2, Length[r_timesZ]}, {{step, 1}, {1, 2, 5, 10, 50, 100, 200}}}]},
           Manipulate[
            lowWeightFrom = 100;
          simdataZ = SimPamFZ[#, args] & /@ r_timesZ;
            plotdataZ = Transpose[{r_timesZ, simdataZ}];
            resdataZ = r_rawdataZ - simdataZ;
            resplotdataZ = Transpose[{r_timesZ, resdataZ}];
            ListPlot[{Transpose[{r_timesZ, r_rawdataZ}][[Floor[xFrom] ;; Floor[xTo]]], plotdataZ[[Floor[xFrom] ;; Floor[xTo]]], resplotdataZ[[Floor[xFrom] ;; Floor[xTo]]]},
             PlotRange → {All, {-0.1, 0.7}}, ImageSize → {580, 520}, PlotMarkers → Graphics@{Disk[{0, 0}, Scaled@0.003]}, Joined → {False, True, False}, PlotStyle → {{Orange}, {Red, Thick}, Gray},
             PlotTheme → "Detailed", FrameLabel → {"Time (s)", "Rel. ChlF Yield. (a.u.)"}, BaseStyle → {FontSize → 18}, Frame → {True, True, True, True},
             PlotStyle → Directive[Thick, Black, PointSize[Large]]], Evaluate[Grid[Transpose[Map[Control, Partition[controls, 17], {-3}]]], ControlPlacement → Right, ContentSize → {640, 550}]]
```

Out[223]=

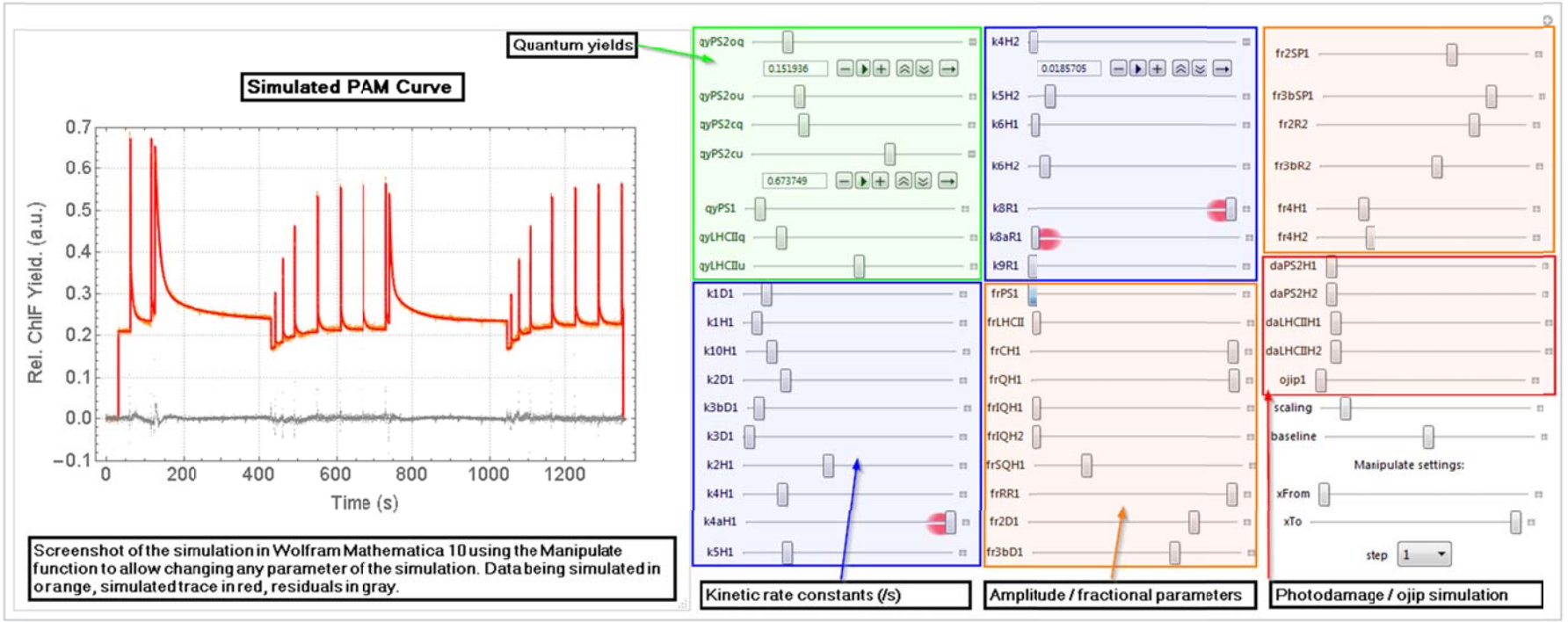

Figure S 2: Annotated screenshot of the simulation of the Z data in Wolfram Mathematica 10. The simulation function is underlined in red and takes as arguments: element out of a list of timepoints (r_timesZ) and arguments for which the controls are shown to the right of the graphics. Note that the variables named differ slightly from those in the main text (most notably k4aH1 = $k_{4a}^{H1} = k_{SQ}^{H1}$), and not all variables are directly relevant for the simulation shown (for instance none of the parameters related to simulating photodamage or different OJIP dynamics are used).

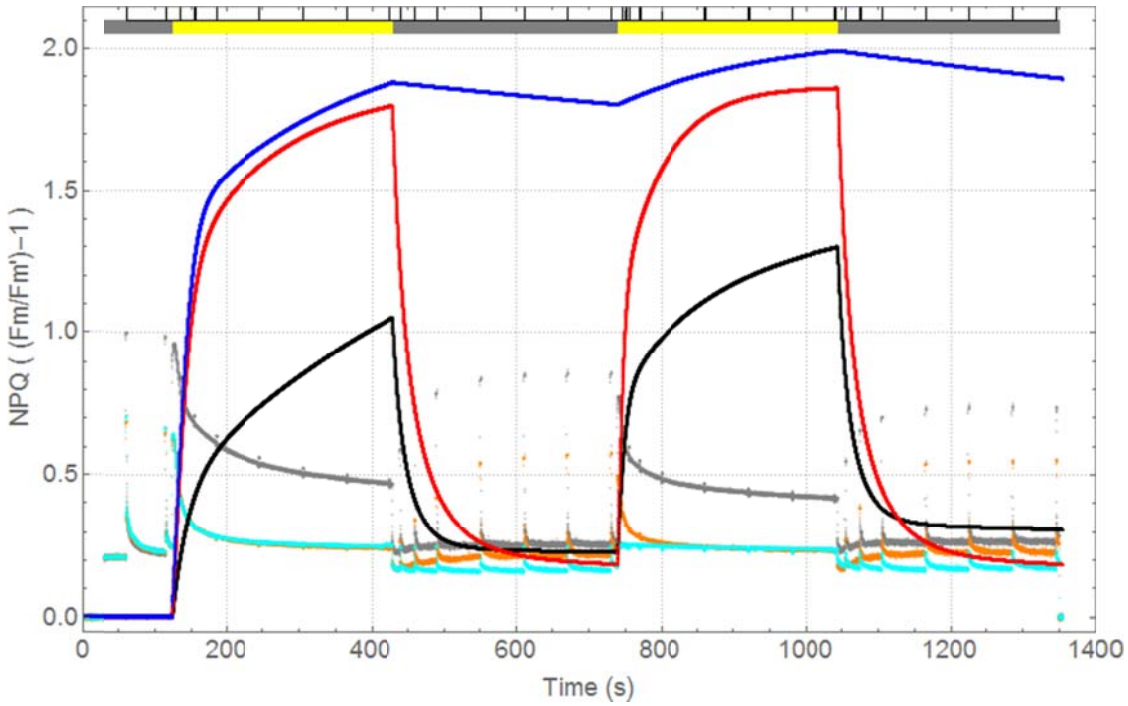

Figure S 3. Level of NPQ (defined as: Fm/Fm' -1) during a fluorescence quenching analysis experiment on intact Chloroplasts devoid of zeaxanthin (black, labeled 'V') or enriched in zeaxanthin (red ('Z'), blue ('GA')). The blue curve represents a sample where glutaraldehyde (GA) was added (at t≈410s) to prevent the recovery from the quenched state. The level of NPQ is calculated directly from the fitting function with the kinetic parameters that describe the decay following a saturating pulse set to zero (i.e. continuously in Fm'). In the background the original data from **Figure 2** of the main text is shown: the V dataset in gray, the Z dataset in orange and the GA dataset in cyan. Light conditions indicated by the top bar as described in the caption of that figure.

The NPQ parameter is a commonly used derived quantity. It is expressed as (Fm/Fm'-1), where Fm is the maximal fluorescence during a saturating pulse in darkness, or alternatively the maximum reached directly after switching on actinic light after a period of dark adaptation, and Fm' the maximal fluorescence reached in a saturating pulse during actinic light exposure. In the context of the functions listed in **Table S 1** and defined above, Fm can be defined as the maximum of the functions labeled "dkspR" or "dk2hl", and Fm' can be defined as the "hlspD" function evaluated with all decay rates set to zero (so that the level stays at the maximum of the "hlspR" function). In the recovery period instead of "hlspD" the function "recspD" is used. In **Figure S 3** the NPQ curves for all datasets are visualized.

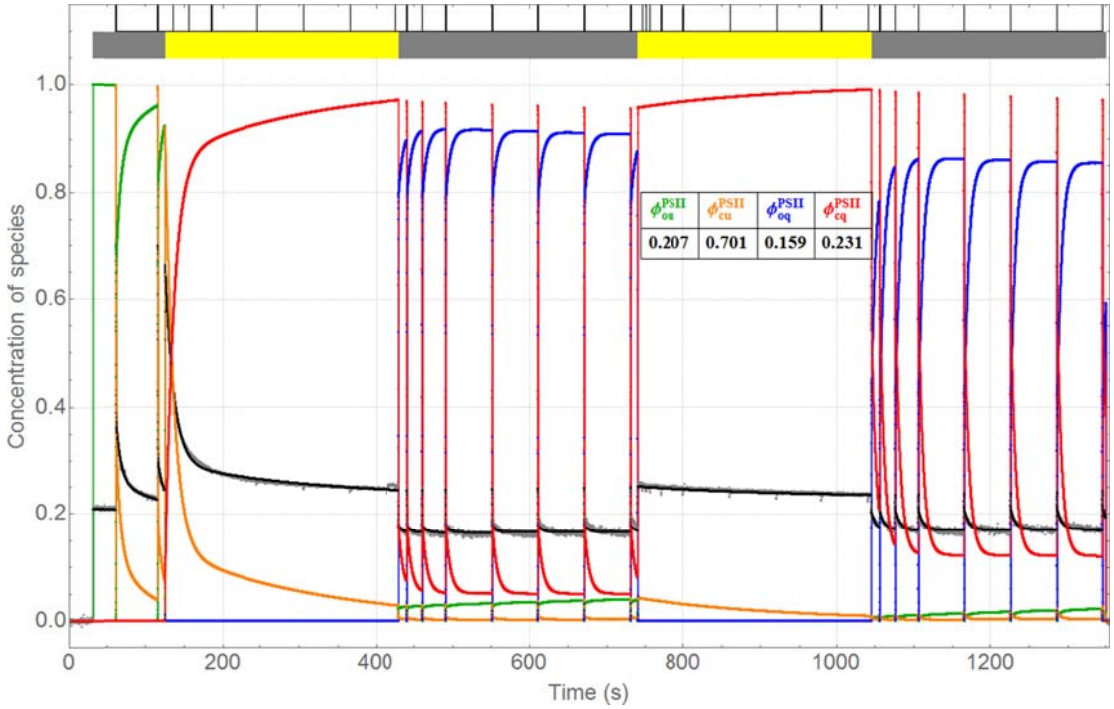

Figure S 4: Concentration profiles of the different states of PSII contributing to the total relative chlorophyll fluorescence quantum yield for the GA dataset. The sum of the concentrations, open unquenched PSII (green, $\Phi_{ou}^{PSII} = 0.207$), closed unquenched PSII (orange, $\Phi_{cu}^{PSII} = 0.701$), open quenched PSII (blue, $\Phi_{cq}^{PSII} = 0.159$) and closed quenched PSII (red, $\Phi_{cq}^{PSII} = 0.231$) multiplied by their respective quantum yields produce the PAM curve depicted in solid black. For comparison the GA observations are overlaid as gray dots. Light conditions indicated by the top bar as described in the caption of **Figure 2**.

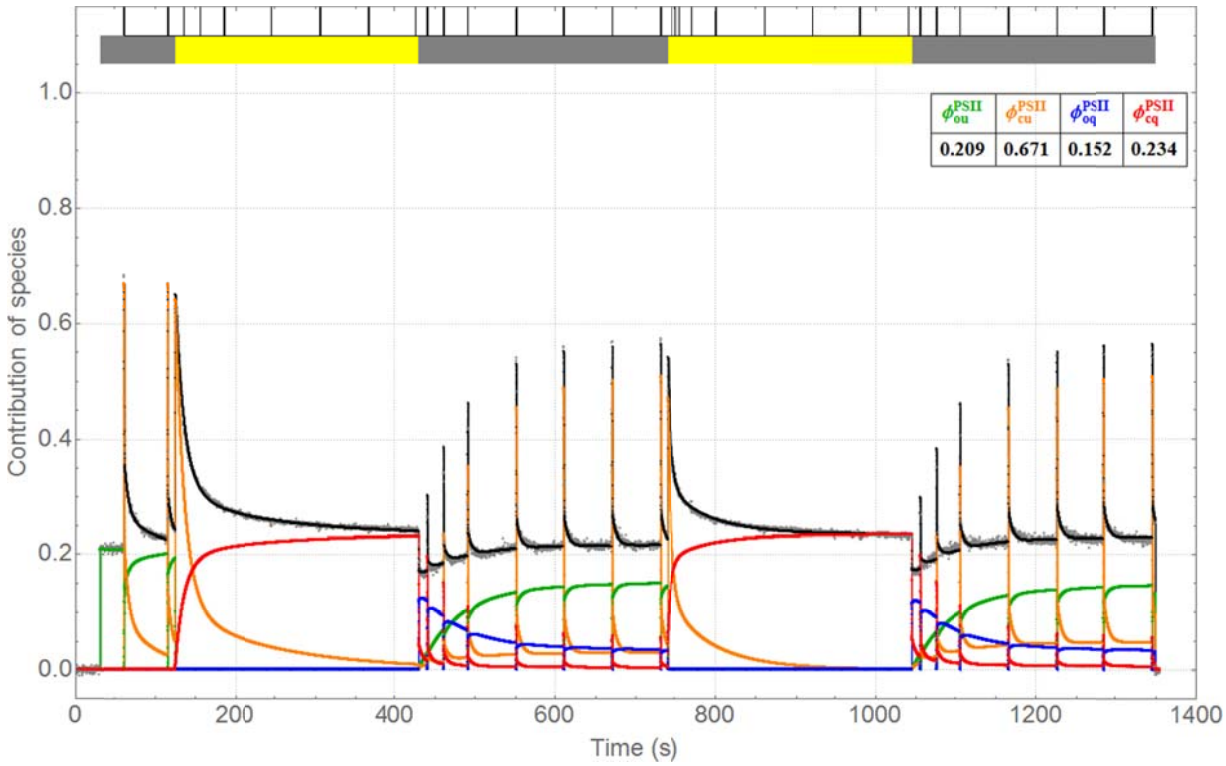

Figure S 5. Contributions of the different states of PSII to the total relative chlorophyll fluorescence quantum yield for the Z dataset. The contribution of a PSII state is defined as the product of its concentrations (shown in **Figure 7**) and the relative quantum yields: open unquenched PSII (green, $\Phi_{ou}^{PSII} = 0.209$), closed unquenched PSII (orange, $\Phi_{cu}^{PSII} = 0.671$), open quenched PSII (blue, $\Phi_{oq}^{PSII} = 0.152$) and closed quenched PSII (red, $\Phi_{cq}^{PSII} = 0.234$). The total fitted contribution is in solid black, observations depicted as gray dots. Light conditions indicated by the top bar as described in the caption of **Figure 2**.

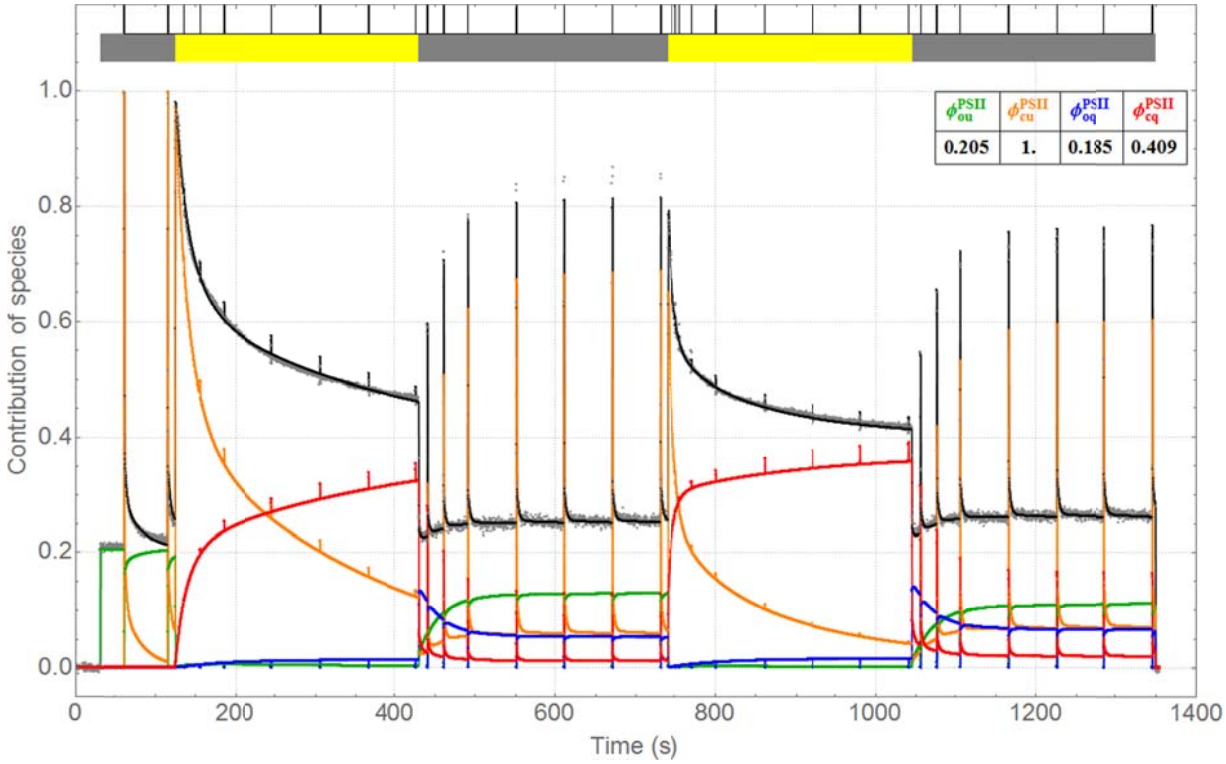

Figure S 6 Contributions of the different states of PSII to the total relative chlorophyll fluorescence quantum yield for the V dataset. The contribution of a PSII state is defined as the product of its concentrations (shown in **Figure 8**) and the relative quantum yields: open unquenched PSII (green, $\Phi_{ou}^{PSII} = 0.205$), closed unquenched PSII (orange, $\Phi_{cu}^{PSII} = 1$), open quenched PSII (blue, $\Phi_{oq}^{PSII} = 0.185$) and closed quenched PSII (red, $\Phi_{cq}^{PSII} = 0.409$). The total fitted contribution is in solid black, observations depicted as gray dots. Light conditions indicated by the top bar as described in the caption of **Figure 2**.

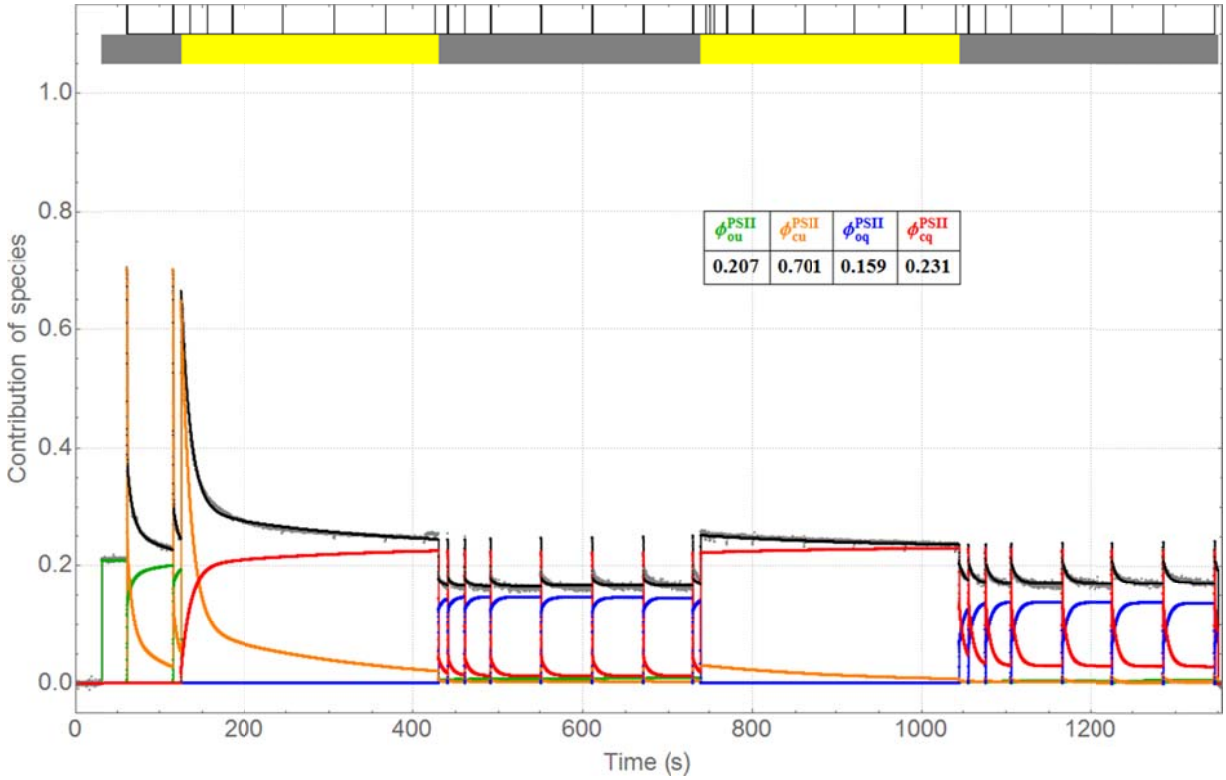

Figure S 7 Contributions of the different states of PSII to the total relative chlorophyll fluorescence quantum yield for the GA dataset. The contribution of a PSII state is defined as the product of its concentrations (shown in Figure S 4) and the relative quantum yields: open unquenched PSII (green, $\Phi_{ou}^{PSII} = 0.207$), closed unquenched PSII (orange, $\Phi_{cu}^{PSII} = 0.701$), open quenched PSII (blue, $\Phi_{oq}^{PSII} = 0.159$) and closed quenched PSII (red, $\Phi_{cq}^{PSII} = 0.231$). The total fitted contribution is in solid black, observations depicted as gray dots. Light conditions indicated by the top bar as described in the caption of **Figure 2**.

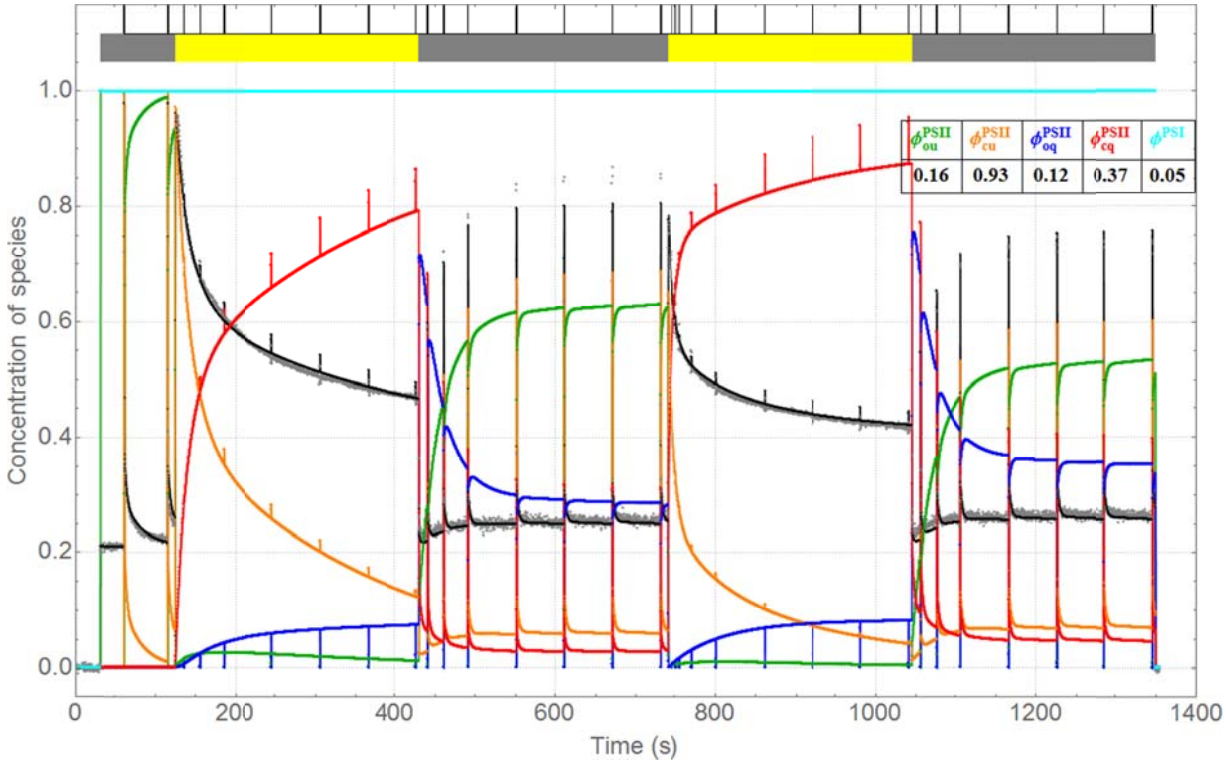

Figure S 8. Concentration profiles of the different states of PSII **and PSI** contributing to the total relative chlorophyll fluorescence quantum yield for the V dataset. The sum of the concentrations, open unquenched PSII (green, $\Phi_{ou}^{PSII} = 0.16$), closed unquenched PSII (orange, $\Phi_{cu}^{PSII} = 0.93$), open quenched PSII (blue, $\Phi_{oq}^{PSII} = 0.12$), closed quenched PSII (red, $\Phi_{cq}^{PSII} = 0.37$) and PSI (cyan, $\Phi^{PSI} = 0.05$) multiplied by their respective quantum yields produce the PAM curve depicted in solid black. For comparison the V observations are overlaid as gray dots. Light conditions indicated by the top bar as described in the caption of **Figure 2**.

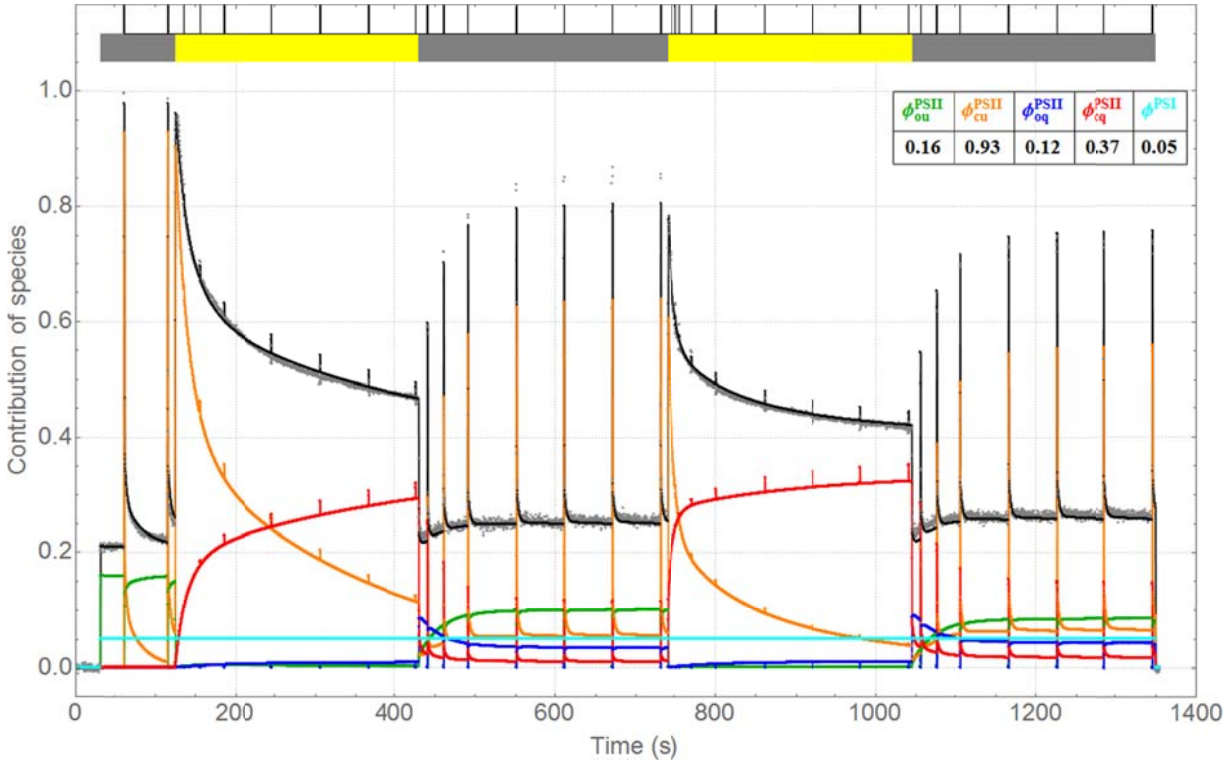

Figure S 9. Contributions of the different states of PSII and PSI to the total relative chlorophyll fluorescence quantum yield for the V dataset. The contribution of a PSII state is defined as the product of its concentrations (shown in Figure S 8) and the relative quantum yields: open unquenched PSII (green, $\Phi_{ou}^{PSII} = 0.16$), closed unquenched PSII (orange, $\Phi_{cu}^{PSII} = 0.93$), open quenched PSII (blue, $\Phi_{oq}^{PSII} = 0.12$), closed quenched PSII (red, $\Phi_{cq}^{PSII} = 0.37$) and PSI (cyan, $\Phi^{PSI} = 0.05$). The total fitted contribution is in solid black, observations depicted as gray dots. Light conditions indicated by the top bar as described in the caption of **Figure 2**.

The link with time-resolved fluorescence spectroscopy

The link with ultrafast time-resolved fluorescence spectroscopy will be established by demonstrating how a target model applied to time-resolved measurements can provide independent estimates of the quantum yields, which can then be compared to those estimated from the quantitative model for PAM fluorometry.
In contrast, ultra-fast time-resolved fluorescence spectroscopy data carries a wealth of information on the picosecond to nanosecond timescales and provides detailed information on the spectral-temporal excited state dynamics upon photo-excitation. However, the experiments are relatively more difficult, take more time and the equipment is costly and cannot easily be carried into the field. Also, putting the system in a particular physiologically relevant condition (quenched, unquenched, closed or open reaction centers (RCs)) and keeping it there for the duration of the measurement is experimentally challenging.
Ultimately however, PAM fluorometry and ultrafast time-resolved fluorescence spectroscopy can be used to probe the same system and both record information on the fluorescence yield, so it should be possible to relate the two experimental techniques to arrive at a more quantitative interpretation of PAM fluorometry curves and potentially bring physiologically relevant parameters to aid in modelling the ultrafast time-resolved fluorescence data using target analysis [2].

Crucial to the decomposition method is the assumption that the measured yield is a superposition of contributions from several species each with their own distinct quantum yield. In intact chloroplasts of plants the general assumption is that the measured yield is due to changes in the efficiency of the photochemistry of PSII, and in line with this assumption so far we have neglected the contribution of PSI. Sometimes the contributions from PSI or disconnected and/or aggregated LHCII antenna need to be taken into account, e.g. in measurements on plants treated with lincomycin which dramatically increases the ratio of antenna per reaction center [3]. For an accurate and quantitative description of the PAM curve good estimates for the relevant quantum yields are necessary, insofar as they cannot be directly estimated from the measured data. In principle the quantum yield can be most accurately estimated from a target analysis of time-resolved spectroscopy data but this requires careful ultra-fast time-resolved measurements in the same conditions as with the PAM measurement. For the V and the Z samples shown in **Figure 2** time-resolved fluorescence data obtained using time-correlated single photon counting (TCSPC) were available [4] which have been re-analyzed using target analysis. Specifically measurements on two states for each of the two samples for a total of four datasets were included in a simultaneous target analysis: closed unquenched ('Fm') and closed quenched ('NPQ') for the sample devoid of Zeaxanthin (VFm, VNPQ) and for the sample enriched in Zeaxanthin (ZFm, ZNPQ) (see also Figure 1). The state of the PSII RCs in the four datasets is assumed to be completely closed for all datasets and either unquenched or fully quenched. Excitation occurred at 470 nm, predominantly exciting Chl b and Carotenoid, and thus relatively more PSII than PSI.

The datasets were first globally analyzed individually, i.e. each dataset represented by a matrix $\Psi(t,\lambda)$ was fitted to the minimal number n_{comp} of exponential decays convolved with an instrument response function (IRF) required to satisfactorily fit the data up to the noise ξ. For each wavelength the amplitude parameters of all exponential decays are determined using the method of variable projection [5] as implemented by the free software TIMP [6] and Glotaran [7]. This results in a decay associated spectrum (DAS) for each component. This can be summarized as:

$$\Psi(t,\lambda) = \sum_{l}^{n_{comp}} \left[\left(\exp[-k_l t] \otimes \mathrm{IRF}(t) \right) \mathrm{DAS}_l(\lambda) \right] + \xi(t,\lambda) \qquad \text{Eq.S29}$$

where k_l is the rate of decay of each component, the reciprocal of which represents the lifetime corresponding to that decay. For each measurement the IRF was independently measured by scattered laser light. Each IRF was characterized by means of a primary Gaussian shaped band, and a number of extra Gaussians shaped bands related to the primary band by a certain scaling factor, a shift in time and a different width. In this way the non-Gaussian nature of the IRF of the TCSPC detector could be very well approximated while maintaining the advantages that a purely analytical model function provides [2] in contrast to numerically convolving the measured IRF with the exponential decays. When fitting the data, all instrument response parameters were fixed except for the position of

the primary Gaussian band which was a free parameter of the fit. This is almost always necessary because the IRF is typically measured at a different wavelength than where the data is measured so there might be a small shift due to dispersion and experimental variation might induce an additional shift. The estimated lifetimes and their Decay Associated Spectra (DAS) are depicted in Figure S 10.

Six components were needed to describe each dataset up to the noise level. The fastest lifetime is shorter than can reliably be estimated given the IRF width (≈110 ps FWHM) but is necessary to account for a bit of relaxation from slightly more blue to redder Chl's in the first tens of ps of the experiment due to a selective excitation of Chl b. The first lifetime that can reliably be resolved is around 0.07-0.1 ns and has a broad emission band peaking around 710 nm, which can safely be attributed to PSI emission. In the ZNPQ datasets this component is likely capturing a small fraction of fast quenching. The next three lifetimes all feature a very similar spectral shape with emission around 680 nm reflecting emission from the LHCII-PSII supercomplex. Clearly quenching is playing a major role on these timescales, differently affecting the samples. The last lifetime represents a tiny fraction of very long lived emission which is observed as a result of measuring for 50 ns. This component likely represents some recombination fluorescence which can safely be ignored. On the basis of one fast component emitting around 710 nm (black DAS) and three DAS with similar shapes (red, blue and magenta) emitting around 680 nm a target model can be constructed consisting of a PSI compartment in parallel to a LHCII-PSII contribution.

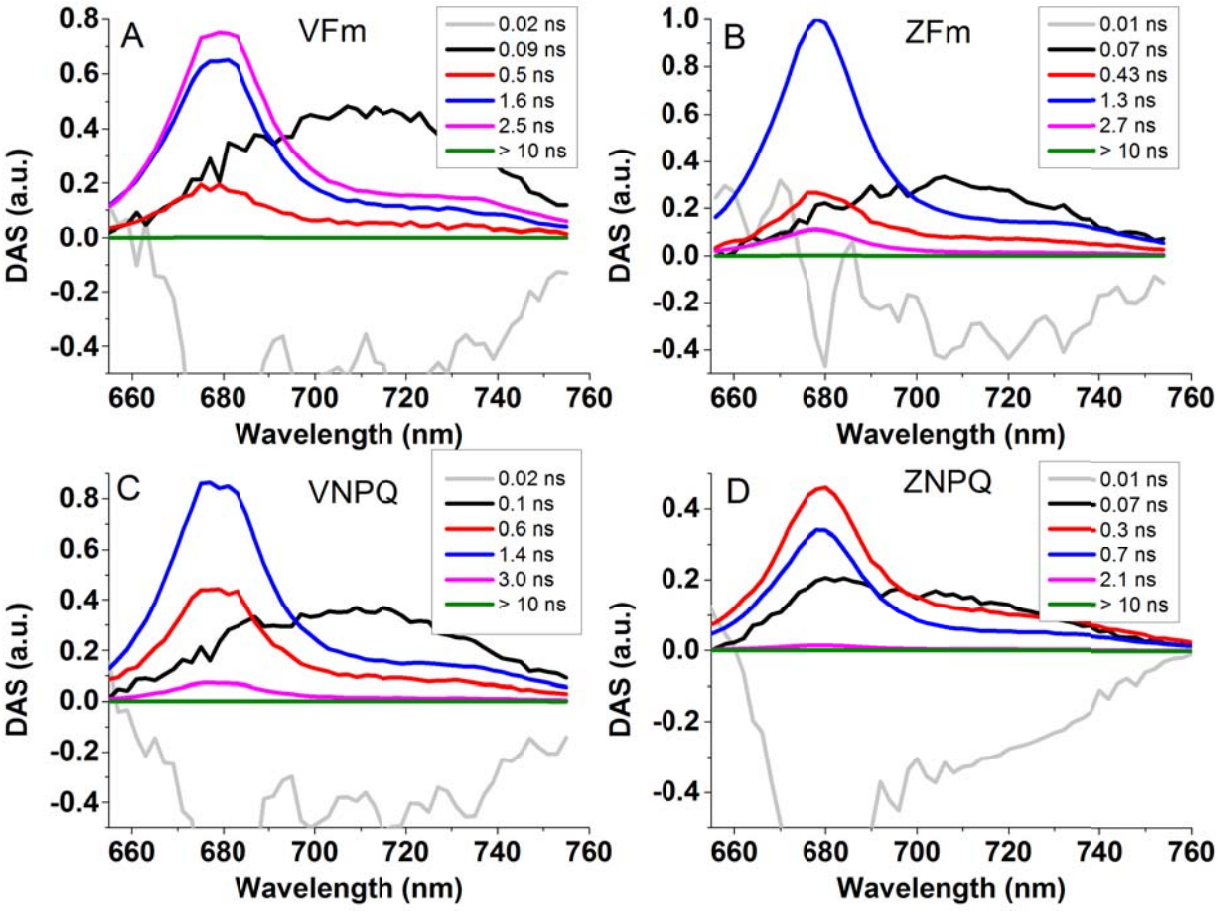

Figure S 10: Global analysis results of the SPC measurements. For the two samples, V and Z as described earlier, two conditions analog to the PAM measurement were probed: closed unquenched ('Fm') and closed quenched ('NPQ'). Shown are the decay associated spectra (DAS) with the estimated lifetimes in the legends. Spectra are normalized to the maximum of the first DAS, except in the case of ZFm where the 4th DAS had the largest amplitude.

Target analysis result

From the global analysis results it is not possible to directly obtain the quantum yield parameters that can be related to the PAM fluorometry data, but it serves as a starting point for a more detailed target analysis which takes into account the different contributions originating from LHCII-PSII and PSI and the different levels of quenching.

To account for the observation of three lifetimes with a similar spectral shape a LHCII-PSII compartment is placed in equilibrium with two (dark) radical pair states, i.e. assuming reversible charge separation, see Figure S 11A. The LHCII-PSII compartment is assumed to be fully equilibrated within the duration of the IRF. The only difference in the model between the four datasets was the quenching rate Q from LHCII-PSII (shown in Figure S 11B) and the shape of the Species Associated Spectra (SAS, c.f. Figure S 11D).). The spectral freedom was needed because the SAS of the LHCII-PSII compartment in the V datasets was less peaked than in the Z datasets irrespective of the Fm or NPQ condition. No evidence was found for an additional quenching site, e.g. in the form of detached LHCII as recently reviewed in [8].

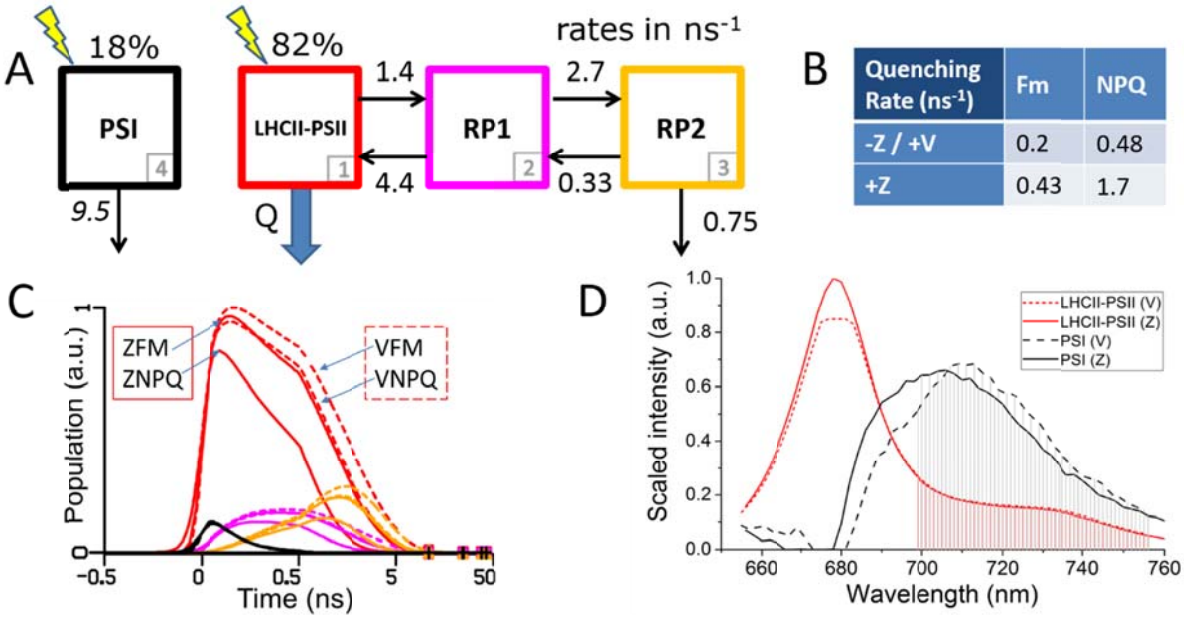

Figure S 11: Overview of simultaneous target analysis results on the four datasets. (A) Target model for time-resolved emission from Chloroplasts at RT excited at 470 nm. All rates (in 1/ns) are fitted parameters with 10% standard error. The input percentages are estimated from an equal SAS area constraint [9]. (B) The quenching rate indicated by Q in the target model for the four different datasets. (C) The population profiles of the different components of the target model. The time axis is linear from -0.5 to 0.5 ns and logarithmic thereafter. (D) The SAS corresponding to the target model for the V datasets (solid) and the Z datasets, with the spectra linked between the Fm and the NPQ state for both. The shading reflects the spectral area used to calculate the relative fluorescence quantum yield as observed by a PAM fluorometer.

Note that whereas in the V samples the quenching rate Q increases from 0.2 in Fm to only 0.48/ns in the NPQ condition, in the ZFm case it is already 0.43/ns. This rate then increases to 1.7/ns in ZNPQ. The quenching is clearly visible in the population profiles in Figure S 11C. Finally the target model can be used to make an estimate for the relative fluorescence quantum yield at the detection wavelengths of the PAM instrument. The steady state concentration levels for each compartment computed from the target analysis are shown in Table S 3.

By multiplying the steady state concentration (which is the integrated area under the population profiles in Figure S 11C) of a fluorescent compartment (i.e. LHCII-PSII, PSI) with the area under its SAS estimated from target analysis (see Figure S 11, panel D), for the relevant integration window of the PAM detector, its relative quantum yield can

be calculated. The calculated quantum yields Φ^{PSII} and Φ^{PSI}, normalized to the yield of PSII in the VFm dataset, can be found in the two rightmost columns of Table S 3.

	LHCII-PSII	RP1	RP2	PSI		φ_{PSII}	φ_{PSI}
VFm	1.402	0.307	0.777	0.019		1.00	0.041
VNPQ	0.913	0.200	0.506	0.019		0.65	0.041
ZFm	0.968	0.212	0.537	0.019		0.68	0.038
ZNPQ	0.379	0.083	0.210	0.019		0.27	0.038

Table S 3: The steady state (integrated) concentrations of the different components in the target analysis depicted in Figure S 11, and the relative quantum yields for PSII and PSI (excited at 470 nm) calculated by multiplying the steady state concentration with the area under its SAS for the region $700 < \lambda < 755\,\text{nm}$.

The relative estimated quantum yield for PSII between the four different cases is largely independent of the excitation wavelength and can therefore be directly compared with what is estimated from PAM fluorometry data regardless of the measuring light used, but the relative yield between PSII and PSI is dependent on the excitation wavelength and cannot always directly be compared. From Table S 3it can be seen that the contribution of PSI according to this target analysis of time-resolved data excited at 470 nm is on the order of a few percent. In the case of the most heavily quenched sample (ZNPQ) the relative contribution is a bit more than 10%. The PAM data reported in this paper was obtained with 620 nm measuring light thus the relative yields are not necessarily comparable. In other work it has been shown that with 624 nm excitation the contribution of PSI to Fo could be as much as 24% in Arabidopsis leaves [10]. This means that the relative quantum yield of PSI for the PAM data (Φ^{PSI}_{PAM}) could be as much as 24% of 0.2, i.e. $\Phi^{PSI} = 0.05$. Assuming a PSI to PSII stoichiometry of 1:1 the effect of including this contribution of PSI has been investigated and the results for the V dataset are reported in Figure S 8 and Figure S 9. The only effect is a small change in the estimated PSII quantum yields: $\Phi^{PSII}_{ou} = 0.16$, $\Phi^{PSII}_{cu} = 0.93$, $\Phi^{PSII}_{oq} = 0.12$, $\Phi^{PSII}_{cq} = 0.37$, $\Phi^{PSI} = 0.05$. Because PSI contributes only an offset (no closing or quenching dynamics) the data could still be fitted equally well.

At this point it makes sense to compare the quantum yields estimated from PAM fluorometry as shown in Figure 9, Figure 10, and Table 1 with those estimated from the target analysis of time-resolved fluorescence as shown in Figure S 11 and summarized in Table S 3. The quantum yields that could be estimated from both techniques are shown in Table S 4.

Dataset	QY label	rel. yield. SPC	rel. yield. PAM
'VFm'	$\Phi^{PSII,V}_{cu}$	1.00	1.00
'VNPQ'	$\Phi^{PSII,V}_{cq}$	0.65	0.41
'ZFm'	$\Phi^{PSII,Z}_{cu}$	0.68	0.67
'ZNPQ'	$\Phi^{PSII,Z}_{cq}$	0.27	0.23

Table S 4: The relative quantum yields for the different states of PSII as could be estimated from SPC data or PAM data.

The quantum yields estimated via either technique are relative to the quantum yield obtained in the Fm case of the V sample. In the case of the PAM fluorometry measurements this is done by normalizing the data to the maximal level of fluorescence in darkness (Fm) where it can be assumed that the only contribution is PSII closed unquenched. In the case of the time-resolved measurement the integrated contribution of LHCII-PSII in the VFm dataset is defined to be 1, the LHCII-PSII contributions in the other datasets are related to this. In the time-resolved data the quantum yield is corrected for the PSI contribution, meaning a small relative error between the two methods is to be expected. Despite this there is considerable consistency in the estimated quantum yields, except perhaps for the VNPQ case.

However it should be noted here that the limited time-resolution of the TCSPC setup (≈110 ps FWHM) meant that it was not possible to reliably quantify quenching processes faster than this, meaning that in the SPC measurement the quantum yield can easily be overestimated due to underestimating the amount of NPQ taking place at early timescales, whereas the yield estimated from the PAM is a reflection of the true quantum yield. This discrepancy could be further investigated by obtaining time-resolved measurements with a much higher time-resolution, for instance using a streak camera setup [11]. Also from the results of the analysis of the PAM curve for the V dataset presented in Figure 9 it can be seen that making sure that the excitation pressure is high enough to keep all RC continuously closed is challenging. The VNPQ case could reflect a mixture of open/closed as well as quenched/unquenched.

Simulations using the Matuszynska et al. 2016 model

Thanks to the availability of the complete simulation source code of the model [12] it was possible to adapt our own light protocol and use it as input for their model. Note that the model was calibrated for the simulation of PAM fluorometry on *Arabidopsis* leafs and not spinach chloroplast, which might explain some inaccuracies in the prediction. Following the same open source philosophy the source code to reproduce these figures is provided in a supplemental file included with this SI. Below follows a brief description in words.

Read in our own raw data (plain csv file) and extract the column with the V fluorescence trace.
Read in our own light protocol stored as two separate files (json format), one containing the timing information on the saturating pulses and the other containing information about the light regimes. Convert this light protocol to the format required by the model.
Initialize the model (type: 'Arabidopsis') with the default parameters and initialize the simulation.
Integrate the model over the times provided by the light protocol.
Extract the PSII state variables (open: B_0; closed B_2) and the degree of quenching Q(t), required for the plotting.
The simulated fluorescence quantum yield Φ can now be described as the sum of the quantum yield in PSII state 0 (open) Φ_{st0} and PSII in state 2 (closed) Φ_{st2}:

$$\begin{aligned}\Phi_{st0}(t) &= k_F / (k_F + k_H * Q(t) + k_{PQ}) * B_0(t)\\ \Phi_{st2}(t) &= k_F / (k_F + k_H * Q(t)) * B_2(t)\\ \Phi(t) &= (\Phi_{st0}(t) + \Phi_{st2}(t)) / \max(\Phi_{st0} + \Phi_{st2})\end{aligned} \qquad \text{Eq.S30}$$

where k_F is the rate of intrinsic fluorescence decay, k_H is the rate of quenching (dissipated as heat) and k_{PQ} is the rate of photochemistry. The rate of NPQ is given by k_H*Q(t), which is modulated by the quencher activity Q which is in turn dependent on the relative concentration of PsbS [PsbS] and Zeaxanthin [Zx], defined as:

$$\begin{aligned}Q = {} & \gamma_0(1-Z_s)[\mathrm{PsbS}] + \gamma_1(1-Z_s)[\mathrm{PsbS}^P]\\ & + \gamma_2 Z_s[\mathrm{PsbS}^P] + \gamma_3 Z_s[\mathrm{PsbS}]\end{aligned} \qquad \text{Eq.S31}$$

where $Z_s = \dfrac{[Zx]}{[Zx] + k_{ZSat}}$ reflects the contribution of Zx to the quenching and k_{ZSat} is a half-saturation constant. The γ parameters were fitted by [12].

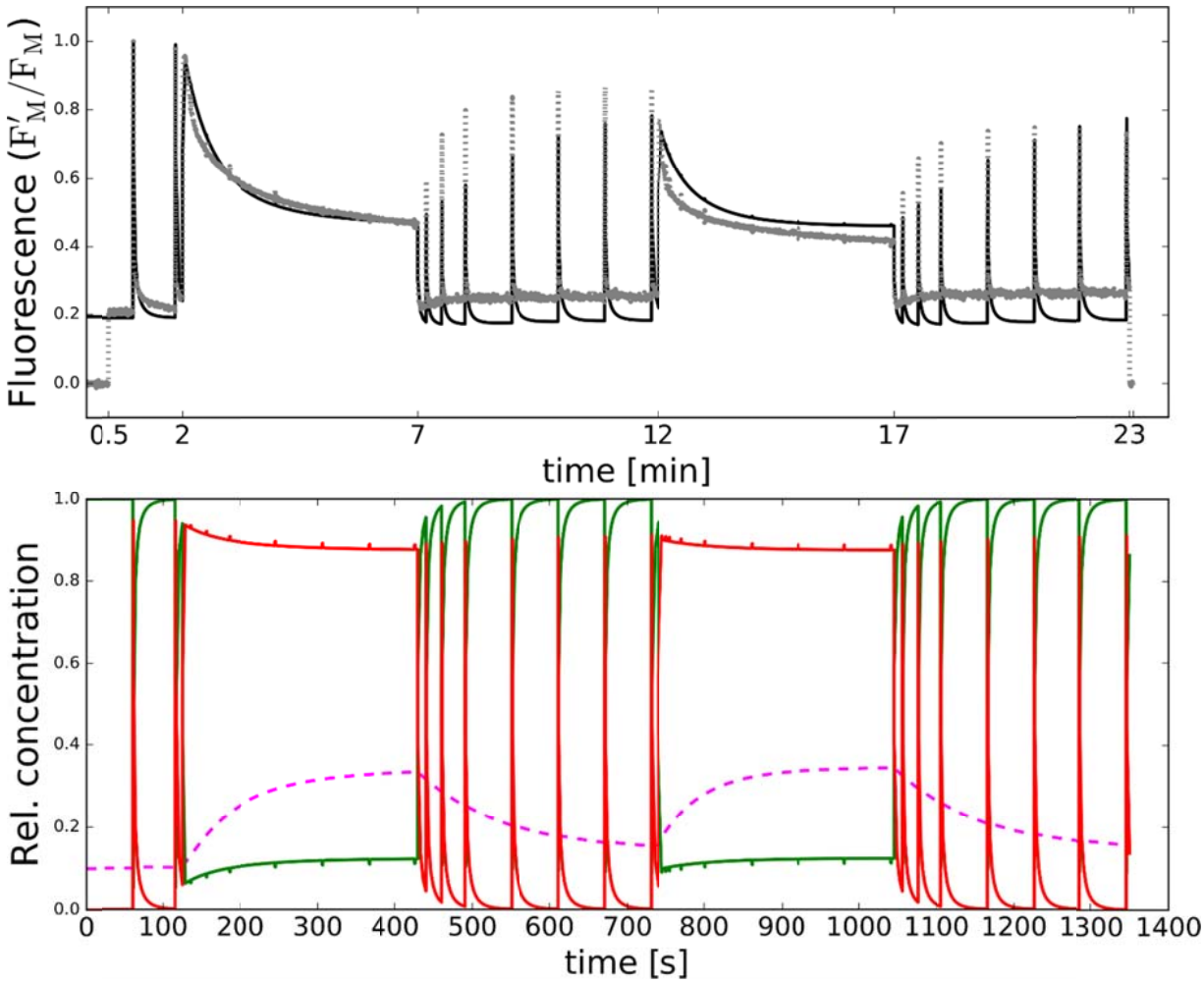

Figure S 12 Predicted fluorescence yield (see Eq.S30) and decomposition using the model published in [12] version 9d46f46 available from https://github.com/QTB-HHU/npqmodel. Top panel shows the predicted fluorescence (solid black) and overlaid the V dataset from Figure 2. Bottom panel shows the decomposition in terms of open PSII (green) and closed PSII (red), in addition the quenching curve Q is shown in magenta.

The clear advantage that an underlying biophysical model provides is that it allows for the investigation of other non-directly observable physical quantities such as the lumenal pH and the relative PsbS and Zeaxanthin concentrations as demonstrated in Figure S 13.

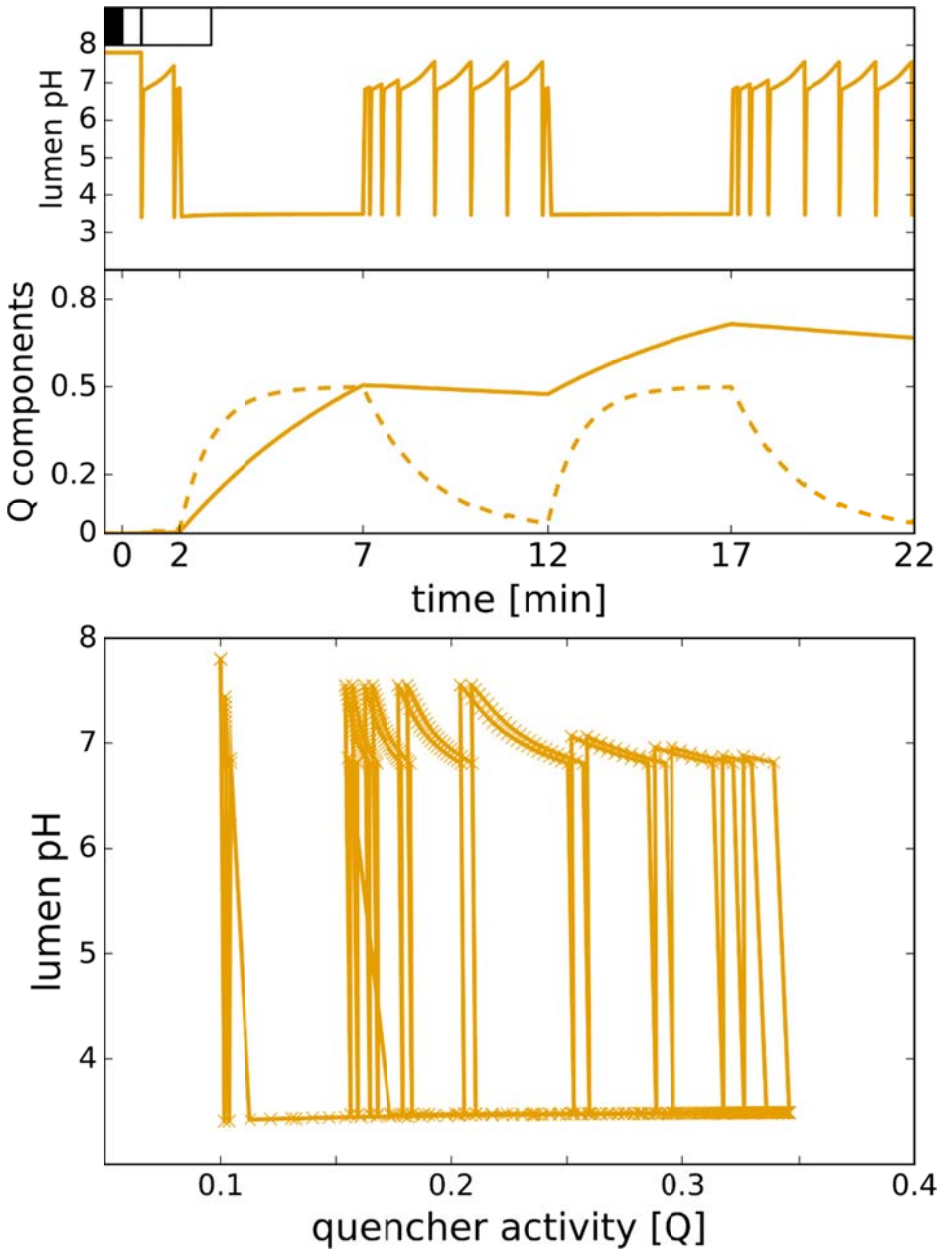

Figure S 13. In analogy to Figure 5 from [12], (top panel) the visualization of lumenal pH changes in the response to our light protocol. (middle panel) the dynamics of the quenching components (solid line for the relative zeaxanthin concentration, dashed line for the ratio of protonated PsbS), (bottom panel) The phase plane trajectories of the quenching variable (Q) and the lumenal pH during our light protocol.

References

[1] A.M. Acuna, J.J. Snellenburg, M. Gwizdala, D. Kirilovsky, R. van Grondelle, I.H.M. van Stokkum, Resolving the contribution of the uncoupled phycobilisomes to cyanobacterial pulse-amplitude modulated (PAM) fluorometry signals, Photosynth Res, 127 (2016) 91-102.
[2] I.H.M. van Stokkum, D.S. Larsen, R. van Grondelle, Global and target analysis of time-resolved spectra, Biochim Biophys Acta, 1657 (2004) 82-104.
[3] E. Belgio, M.P. Johnson, S. Jurić, A.V. Ruban, Higher plant photosystem II light-harvesting antenna, not the reaction center, determines the excited-state lifetime-both the maximum and the nonphotochemically quenched., Biophysical journal, 102 (2012) 2761-2771.
[4] M.P. Johnson, M.L. Pérez-Bueno, A. Zia, P. Horton, A.V. Ruban, The zeaxanthin-independent and zeaxanthin-dependent qE components of nonphotochemical quenching involve common conformational changes within the photosystem II antenna in Arabidopsis., Plant physiology, 149 (2009) 1061-1075.
[5] G.H. Golub, V. Pereyra, The Differentiation of Pseudo-Inverses and Nonlinear Least Squares Problems Whose Variables Separate, SIAM Journal on Numerical Analysis, 10 (1973) 413-432.
[6] K.M. Mullen, I.H.M. van Stokkum, TIMP: An R Package for Modeling Multi-Way Spectroscopic Measurements, Journal of Statistical Software, 18 (2007).
[7] J.J. Snellenburg, S.P. Laptenok, R. Seger, K.M. Mullen, I.H.M.v. Stokkum, Glotaran: A Java-Based Graphical User Interface for the R Package TIMP, Journal of Statistical Software, 49 (2012).
[8] A.R. Holzwarth, P. Jahns, Non-photochemical quenching mechanisms in intact organisms as derived from ultrafast-fluorescence kinetic studies, in: Non-Photochemical Quenching and Energy Dissipation in Plants, Algae and Cyanobacteria, Springer, 2014, pp. 129-156.
[9] J.J. Snellenburg, J.P. Dekker, R. van Grondelle, I.H.M. van Stokkum, Functional compartmental modeling of the photosystems in the thylakoid membrane at 77 K, J Phys Chem B, 117 (2013) 11363-11371.
[10] E.E. Pfündel, C. Klughammer, A. Meister, Z.G. Cerovic, Deriving fluorometer-specific values of relative PSI fluorescence intensity from quenching of F0 fluorescence in leaves of Arabidopsis thaliana and Zea mays, Photosynthesis Research, 114 (2013) 189-206.
[11] I.H.M. van Stokkum, B. van Oort, F. van Mourik, B. Gobets, H. van Amerongen, (Sub)-picosecond spectral evolution of fluorescence studied with a synchroscan streak-camera system and target analysis, in: Biophysical techniques in photosynthesis, Springer, 2008, pp. 223-240.
[12] A. Matuszyńska, S. Heidari, P. Jahns, O. Ebenhöh, A mathematical model of non-photochemical quenching to study short-term light memory in plants, Biochimica et Biophysica Acta (BBA) - Bioenergetics, 1857 (2016) 1860-1869.